- Technical Paper -

DYNAMIC RESPONSE ANALYSIS OF RC SLABS WITH VARIOUS SUPPORT CONDITIONS UNDER IMPACT LOADING

Dandan ZHENG[*1], Masato KOMURO[*2], Norimitsu KISHI[*3] and Yusuke KURIHASHI[*4]

ABSTRACT

In this study, 3D elasto-plastic dynamic response analyses were conducted on rectangular reinforced concrete slabs with various support conditions under impact loading. An applicability of an FE model proposed here was investigated comparing with the experimental results. The results obtained from this study were as follows: 1) configurations of the time histories of the impact force, reaction force, and deflection can be better predicted irrespective of the support conditions; and 2) major crack patterns can be approximately simulated for all cases by means of the proposed method.

Keywords: RC slab, impact loading, dynamic response, elasto-plastic numerical analysis

1. INTRODUCTION

In recent years, due to a variety of natural disasters such as global warming, a number of damage events on rockfall protective structures such as RC rock-sheds, steel wire nets and fences have increased. At present, the structural design for these RC structures has been carried out on the basis of the "allowable stress" design concept. However, the design concept for infrastructures tends to be shifted from "allowable stress design method" to "performance-based design method" through "limit state design method".

In order to establish the performance-based design method for impact resistant structures, a lot of experiments have been done to accumulate the fundamental knowledge on impact resistant behavior of these members and/or structures. However, it is very difficult to conduct many experimental studies because of their high cost. Therefore, to achieve this goal more efficiently, numerical analysis studies should be conducted. The authors have proposed a numerical analysis method using an FE model with a simple constitutive law model [1] for concrete. An applicability of the proposed method was mainly verified for 1D structural members such as RC beams and/or girders [2-5].

From this point of view, in this study, to investigate an applicability of the proposed method for 2D structures such as slabs and/or walls under impact loading, 3D elasto-plastic dynamic response analyses

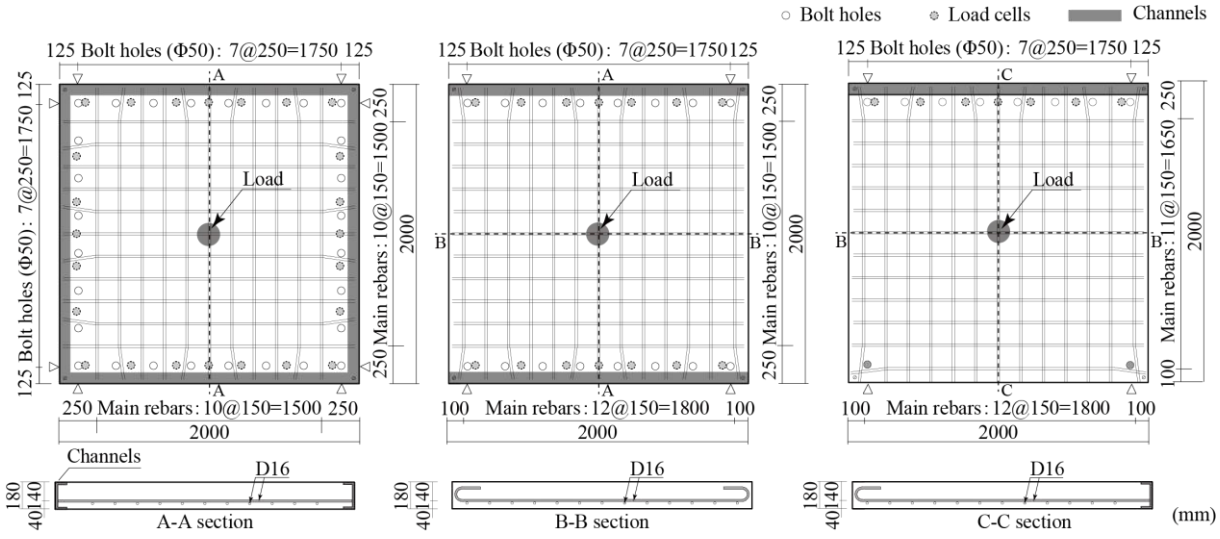

(a) Slab S4 (four-side supported) (b) Slab S2 (two-side supported) (c) Slab S1 (one-side and two-point supported)

Fig. 1 Dimensions and reinforcement layouts of rectangular RC slabs

*1 Ph.D. Student, Division of Engineering, Muroran Institute of Technology, JCI Student Member
*2 Associate Prof., Dept. of Civil Engineering, Muroran Institute of Technology, Dr. E., JCI Member
*3 Emeritus Prof., Muroran Institute of Technology, Dr. E., JCI Member
*4 Lecturer., Dept. of Civil Engineering, Muroran Institute of Technology, Dr. E., JCI Member

Table 1 Experimental cases

Type	Support conditions	Depth (mm)	Impact velocity (m/s)	Compressive strength (MPa)
S4	Four-side	180	4.0,4.5	26.3
S2	Two-side			26.2
S1	One-side and two-point			27.3

were conducted for rectangular reinforced concrete (RC) slabs. The applicability of the method was investigated comparing between numerical and experimental results [6]. In this study, total six cases with different support conditions were analyzed taking impact velocities of the striker as variables. Here, LS-DYNA [7] commercial program (ver. R9) was used.

2. OUTLINE OF EXPERIMENTS

2.1 Dimensions of RC slabs

Figure 1 shows the dimensions and reinforcement layouts of the rectangular RC slabs used in this study. Dimensions of the slabs were 2,000 × 2,000 × 180 mm (width × length × depth) and both clear spans were 1,750 mm. Deformed rebars of diameter φ = 16 mm were placed every 150 mm in two directions, and the average depth of concrete cover was 40 mm. The anchorage methods of steel rebars were varied corresponding to the support conditions as shown in Fig. 1. For simple supported edge of the slabs S4, S2 and S1, main rebars were welded to channels at the end of slabs to save the anchorage length. For free edge of the slabs S2 and S1, the ends of main rebars were bent and fixed on the compression sides of slabs.

Experimental cases used in this study were listed in Table 1. In this study, six specimens were prepared with three kinds of support conditions and different impact velocities of the striker. In this table, nominal names of the specimens were designated by support condition (S4: four sides supported; S2: two sides supported; and S1: one side and two points supported). The compressive strength of concrete was also listed in Table 1 obtained from compressive tests.

2.2 Experimental procedure and measuring items

Photo 1 shows an example of the experimental setup for slab S4. Falling-weight impact tests were conducted by dropping the steel-weight (mass: 300 kg) from a prescribed height onto the center of the slab only once. The weight was made of a steel solid cylinder of 1.4 m height and the striking part is 90 mm in diameter as shown in the photo 1. The impacting face was tapered with a height of 2 mm to prevent one-sided contact.

RC slabs were set on the supporting points and fixed through bolts and nuts to prevent the ends of slab lifting off. Only rotation at the bottom of supporting apparatus was allowed while the horizontal movement was restrained.

The measurement items of this experiment were: 1) the impact force measured by using the load-cell embedded in the striker, 2) the total reaction force (hereinafter, reaction force) estimated by measuring load-cells installed in supporting apparatus, and 3) the deflection of the lower surface at the loading point (hereinafter, deflection) measured by using non-contact laser type linear variable displacement transducers. The crack patterns on the bottom side of slabs were also sketched after the experiment.

Photo. 1 Experiment setup (S4 slab)

3. OVERVIEW OF NUMERICAL ANALYSIS

3.1 FE model

Figure 2 shows the finite element models of reinforced concrete slabs with various support conditions used in this study. Here, due to the symmetry, only one-quarter of RC slab including the striker and supporting apparatus was modeled for the slab S4 and S2, and only half of RC slab was modeled for the slab S1.

In the models, the reinforcements were modeled by using a two-node beam element with 2×2 Gauss points that has equivalent axial stiffness, cross-sectional area, and mass with those of real ones. The channels were modeled by using four-node shell elements, and the others were modeled by using eight-node solid elements with one integration point. Mesh size of FE model was approximately 25 × 25 × 10 mm except for the beam elements. The total numbers of nodal points and elements used in this model were shown in Fig. 2.

In the boundary condition of FE model, the displacement in the normal direction of the symmetry surface was restrained, and only rotation at the bottom of the supporting apparatus was allowed according to experimental conditions. The relationships between concrete and reinforcements, and between concrete and C-shaped channels were assumed to be perfectly bonded to each other. The contact surface model was introduced for interactions between the impact surfaces of concrete and striker, and between concrete and supporting apparatus including bolts and nuts. Friction factor of the contact surface was assumed to be 0.2. Impact load was applied by giving an initial velocity for the whole nodes of the striker placed in contact with RC slab. The impact velocity for each case was listed in Table 1. Damping factor was set to h = 5% for the first natural vibration frequency in the vertical direction based on the preliminary analysis [8].

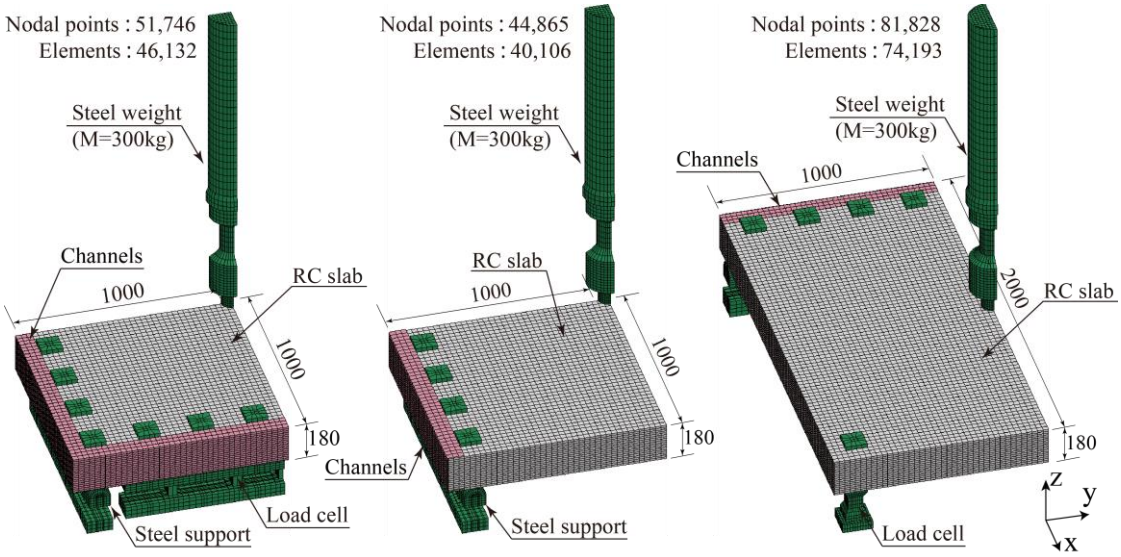

(a) Slab S4 (1/4) (b) Slab S2 (1/4) (c) Slab S1 (1/2)

Fig. 2 Finite element models of slabs

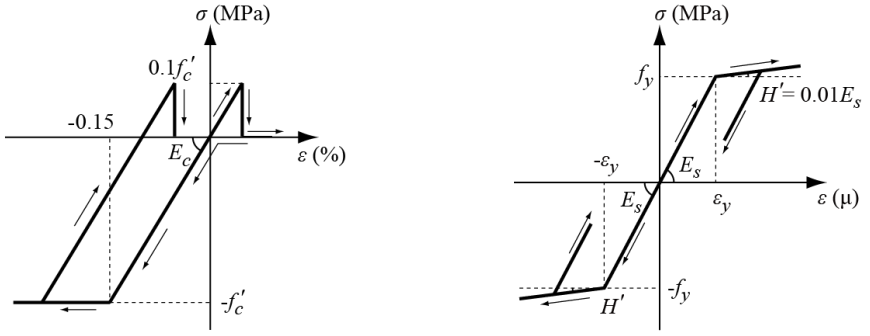

(a) Concrete (b) Reinforcement

Fig. 3 Stress-strain relations of materials

3.2 Material models

Figure 3 shows the stress-strain relationships of concrete and reinforcements used in this study. Strain rate effect was not considered for all materials in this study because the impact velocity of the striker was relatively small. The constitutive law model for each material was briefly described below.

(1) Concrete

Figure 3 (a) shows stress-strain relationships for concrete. The relationship of concrete was defined by an isotropic elasto-plastic model considering the tensile fracture, in which a bilinear model in the compression side and a cutoff model in the tension side were applied. In this model, it was assumed that: (1) concrete was yielded at 0.15 % strains; (2) the tensile stress was interrupted when an applied negative pressure reached the tensile strength of concrete; (3) yield stress was equal to the compressive strength obtained from the test results as listed in Table 1; and (4) the tensile strength was set to be 1/10 of the compressive strength [1]. Yielding of concrete was evaluated using Dracker-Prager's yielding criterion. Internal friction angle of concrete was set to be 30°. The density ρ_c and Poisson's ratio v_c were assumed as $\rho_c = 2.35\times10^3$ kg/m^3 and $v_c = 0.167$, respectively.

(2) Reinforcement

Figure 3 (b) shows the stress-strain relationships for reinforcements. As constitutive model, an isotropic elasto-plastic hardening model considering plastic hardening modulus was applied. The plastic hardening modulus H' was assumed to be 1 % of elastic modulus E_s. Yielding of reinforcing bar was evaluated following von Mises's yield criterion. The yield stress (f_y = 374 MPa) of reinforcing bar was obtained from the coupon test. Material properties: density ρ_s, Young's modulus E_s, and Poisson's ratio v_s were assumed as $\rho_s = 7.85\times10^3$ kg/m^3, E_s = 206 GPa, v_s = 0.3, respectively.

(3) Striker, supports, channels, and load-cells

For the striker, supporting apparatus, channels and load-cells for measuring the reaction force, these were assumed as elastic bodies because no plastic deformation was observed in the experiment. The Young's modulus E_s and Poisson's ratio v_s were set using the nominal value of steel (E_s = 206 GPa, v_s = 0.3). The density ρ_s was assumed as $\rho_s = 7.85\times10^3$ kg/m^3 for the supporting apparatus, channels, and load-cell. The density of the striker was evaluated by dividing mass (300 kg) by volume of the striker.

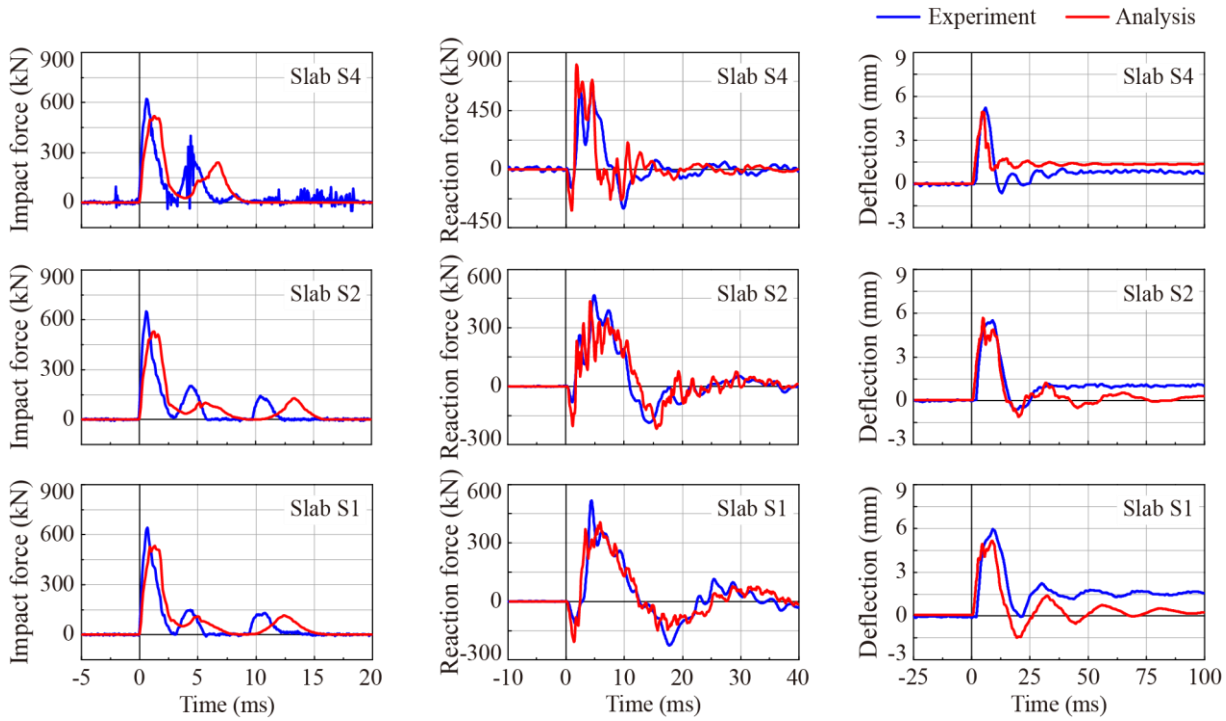

(a) Impact force (b) Reaction force (c) Deflection

Fig. 4 Impact response waves of slabs at the impact velocity V = 4.0 m/s

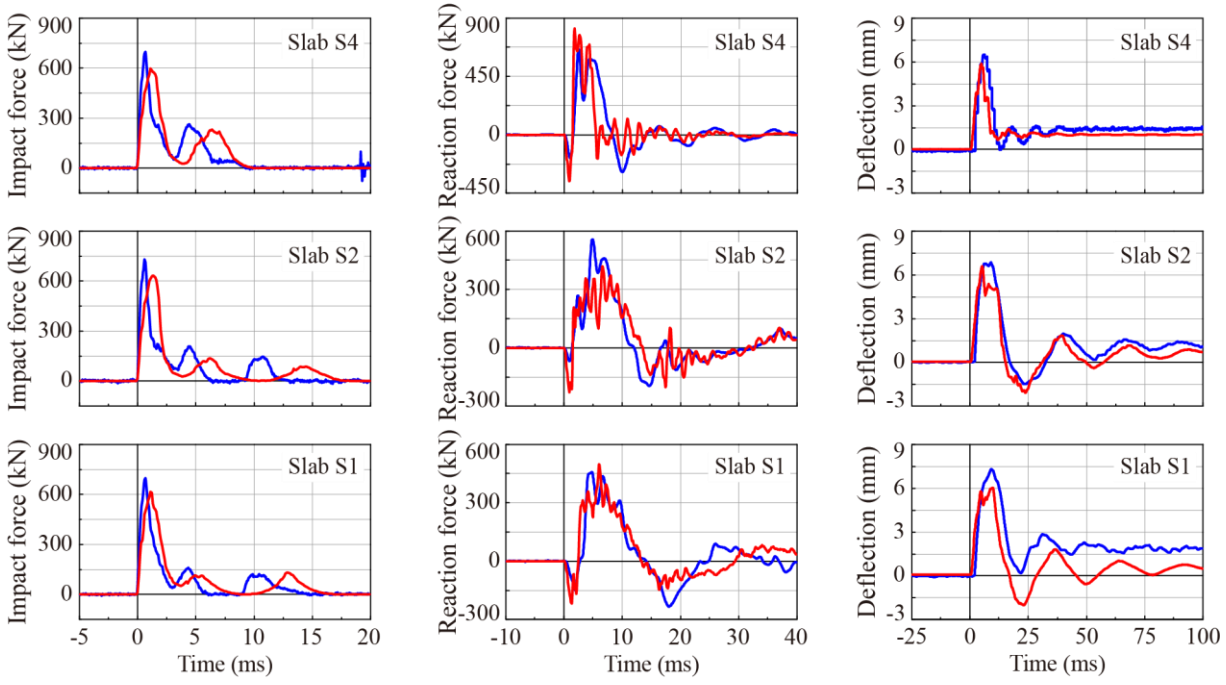

(a) Impact force (b) Reaction force (c) Deflection

Fig. 5 Impact response waves of slabs at the impact velocity V = 4.5 m/s

4. NUMERICAL RESULTS AND DISCUSSIONS

4.1 Time histories of impact force, reaction force, and deflection

Figures 4 and 5 show the comparisons of time histories of (a) impact force, (b) reaction force, and (c) deflection for slab S4, S2, and S1, respectively. In these figures, origin of the time axis was taken as the time when the striker just impacted onto the slab.

Figures 4 (a) and 5 (a) show comparisons of the time histories of impact force between numerical results and experimental results for all cases. From these figures, it is observed that: 1) configurations of the time history of impact forces were composed of a triangular wave

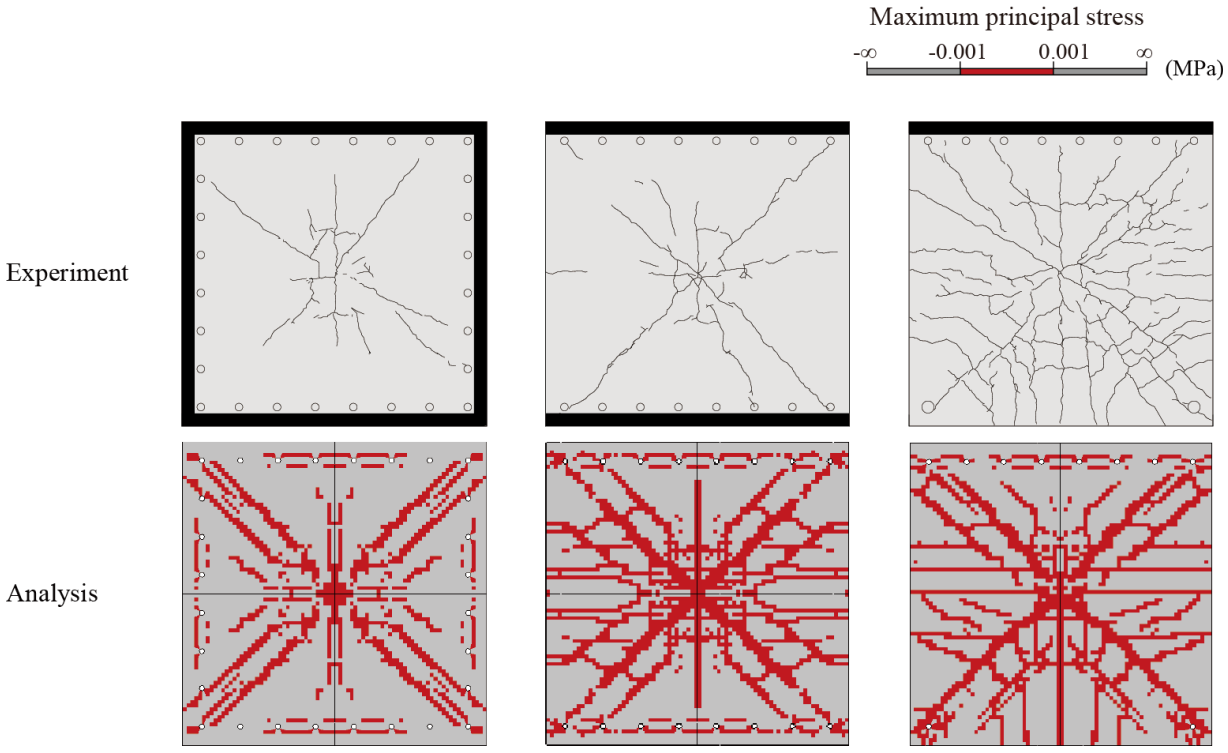

(a) Slab S4 (b) Slab S2 (c) Slab S1

Fig. 6 Crack patterns of slabs at the impact velocity V = 4.0 m/s

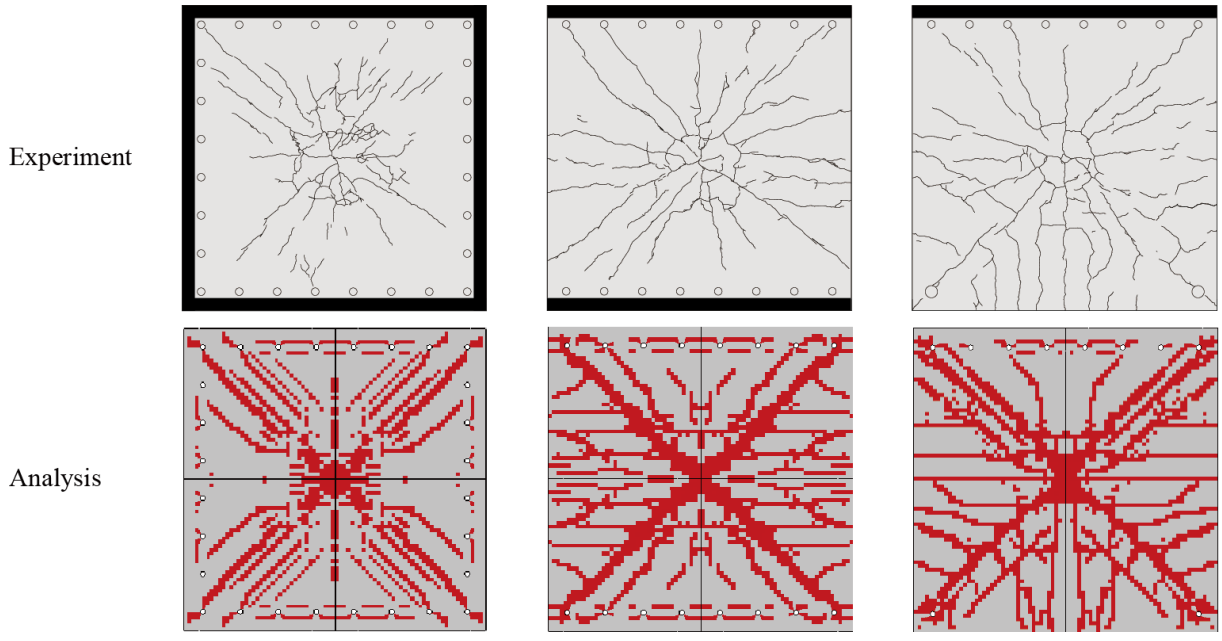

(a) Slab S4 (b) Slab S2 (c) Slab S1

Fig. 7 Crack patterns of slabs at the impact velocity V = 4.5 m/s

with a large amplitude and short duration; 2) maximum impact force was increased with an increment of impact velocity; and 3) maximum impact force under the same impact velocity was almost similar to each other irrespective of the supporting condition of RC slab.

From the comparison between experimental and numerical results, it is seen that: 1) maximum impact forces obtained from the numerical analyses were smaller than those of the experimental results; and 2) however, configuration of the time history was comparatively similar to each other for all cases.

Figures 4 (b) and 5 (b) show comparisons of the time history of reaction force for all cases. From these figures, it is seen that: 1) maximum reaction force of the

slab S4 was larger than those of the slabs S2/S1 under the same impact velocity; 2) configuration of the time history of reaction forces obtained from the numerical results were similar to those of the experimental results; and 3) maximum amplitude and its duration of the main part were also good agreement with the experimental results.

Figures 4 (c) and 5 (c) show comparisons of the time history of deflection. From the experimental results, following results were obtained: 1) the deflection reached a maximum value at an elapsed time of about 10 ms from the beginning of impact, and after that the slab moved to a state of damping free vibration; 2) maximum and residual deflections were increased with an increase of impact velocity; and 3) maximum displacement of the slab S4 was less than the slabs S2/S1 under the same impact velocity.

From the comparison between experimental and numerical results, it is observed that: 1) configuration of the time history of deflection was almost similar to each other; 2) in the case of slab S1, the residual deflection obtained from the numerical analysis was smaller than that of the experimental result; 3) maximum deflection can be properly estimated for all cases.

4.2 Crack patterns

Adopting the constitutive law model for concrete as shown in Fig. 3a, since the tensile stress will be released when the stress in the concrete elements reaches the tensile strength, the element with zero stress may be cracked or actually exhibit zero stress. Here, applying this idea, crack patterns will be predicted, which were the red regions in Figs. 6 and 7.

Figures 6 and 7 shows comparison of the crack patterns caused on the bottom-surfaces of the slab after the test between experimental and numerical results for all cases. From the experimental results, it is observed that in the case of the slab S4, the crack pattern was composed of the circular-shaped cracks due to punching shear failure and the diagonal cracks from the center to the corner. In the case of the slab S2, the crack patterns were almost similar to those of the slab S4, and additional bending cracks near the mid-span parallel to the supporting edges were observed. In the case of the slab S1, it is seen that the slab was more extensively cracked compared to the other two slabs, and the cracks in the shape of a quarter of circle around the pin supports due to axisymmetric bending were observed.

Comparing crack patterns between numerical and experimental results, it is observed that: 1) the cracks near the supports obtained from the numerical analyses tend to be developed excessively than those of the experimental ones; 2) the circular and diagonal cracks in the case of the slab S4, and the bending cracks parallel to the supporting edges in the case of the slab S2, and one-fourth circular-shaped cracks around the pin supports can be approximately better simulated; and 3) however, since symmetric model was adopted in this analysis, it was impossible to accurately simulate irregular cracks observed in the experiment due to effect of the boundary conditions.

5. CONCLUSIONS

(1) Time histories of the dynamic responses (impact force, total reaction force, and deflection at the loading point) can be better predicted irrespective of the support conditions by means of a proposed FE analysis method;
(2) Maximum reaction force, and maximum and/or residual deflections can be almost predicted; and
(3) Crack patterns of the slabs S4, S2, and S1 can also be appropriately evaluated.

REFERENCES

[1] Kishi, N., Mikami, H., Matsuoka, K., and Ando, T., "Elasto-plastic Impact Response Analysis of RC Beams with Statically Bending Failure Mode," Journal of JSCE, No.619/I-47, 1999, pp. 215-233. [in Japanese]

[2] Bhatti, A.Q., Kishi, N., Okada, S., and Konno, H., "Impact Response Analysis of Large Scale RC Girder with Sand Cushion," Proc. of the JCI, Vol. 28, No. 2, 2006, pp. 871-876.

[3] Kishi, N. and Bhatti, A. Q., "An Equivalent Fracture Energy Concept for Nonlinear Dynamic Response Analysis of Prototype RC Girders Subjected to Falling-weight Impact Loading," International Journal of Impact Engineering, Vol. 37, Issue. 1, 2010, pp. 103-113.

[4] Kawarai, T., Kishi, N., Komuro, M., and Kurihashi, K., "Impact Response Analysis for RC Beam Strengthened with NSM-AFRP Rods," Proc. of the JCI, Vol. 39, No. 2, 2017, pp. 583-588. [in Japanese]

[5] Zheng, D., Komuro, M., Kawarai, T., and Kishi, N., "Impact Response Analysis on Impact Resistant Behavior of Flat RC Beam under Falling-weight," Proc. of the JCI, Vol. 39, No. 2, 2017, pp. 619-624. [in Japanese]

[6] Kishi, N., Mikami, H., Kurihashi, K., "A Proposal of Design Procedures for RC Slabs with Various Supporting Conditions and Thicknesses under Falling-weight Impact Loading," Journal of Structural Engineering. Vol. 59A, 2013, pp. 1025-1036. [in Japanese]

[7] Hallquist, J. O., "LS-DYNA Version R9 User's Manual," Livermore Software Technology Corporation, 2017.

[8] Tamaki, M., Kishi, N., Konno, H., and Kawase, R., "Numerical Study on Effect of Yield Criterion on Impact Resistant Behavior of RC Rectangular Slabs," Proc. of the JCI, Vol. 32, No. 2, 2010, pp. 757-762. [in Japanese]